Application of Optical Nuclear Polarization Enhanced ^{13}C NMR

G. Buntkowsky,*,† W. Hoffmann,‡ Teobald Kupka,§,|| Grazyna Pasterna,§ Maria Jaworska,⊥ and H.-M. Vieth‡

Institut für Organische Chemie der Freie Universität Berlin, Takustrasse 3, D-14195 Berlin, Germany, Institut für Experimentalphysik, Arnimallee 14, D-14195 Berlin, Germany, Institute of Physics, Silesian University, Uniwersytecka 4 Street, PL-40-007 Katowice, Poland, Institute of Polymer Chemistry, Polish Academy of Sciences, Zabrze, Poland, and Institute of Chemistry, Silesian University, Bankowa 14 Street, PL-40-007 Katowice, Poland

Received: January 8, 1998; In Final Form: May 11, 1998

A gain in detection sensitivity of more than 3 orders of magnitude has been achieved in high-resolution solid-state ^{13}C NMR of monocrystalline fluorene doped with acridine by applying optical nuclear polarization (ONP) via excited triplet states to protons and transferring this proton polarization to the ^{13}C nuclei. This sensitivity gain was utilized to measure the angular dependence (rotation pattern) of the ^{13}C NMR lines. In this way the principal values and orientations of all ^{13}C chemical shielding tensors were determined. While the ^{13}C shielding tensor of the bridging methylene group exhibits only a small anisotropy, at the aromatic carbon positions the typical strong anisotropy is observed. All tensors belonging to the same molecule have one principal axis, perpendicular to the molecular plane, in common, showing that in the crystal lattice the fluorene molecule is in a planar configuration. The experimental data are compared to ab initio calculations employing optimized geometries and gauge included atomic orbitals density functional theory (GIAO DFT). The orientations of all calculated tensors are in excellent agreement with the experimental data. On an absolute scale the calculated shielding parameters reproduce the experimental values reasonably well. A significant improvement of the calculated eigenvalues is achieved by shifting the tensors employing data from calculations of benzene and methane.

Introduction

The chemical shielding (CS) and its anisotropy reflect the local bonding structure. Since for a quantitative interpretation a theoretical modeling is necessary, many approaches with different levels of sophistication for calculating CS have been published and experimentally tested on model compounds. These approaches range from the classic self-consistent-field (SCF)[55] and gauge origin independent (GIAO)[27,48] calculations via GIAO ab initio calculations,[18,60] individual gauge for localized orbitals (IGLO),[34,49] localized orbital/localized origin (LORG)[28] calculations, and polarization propagator approximation (PPA)[25] to the recent continuous transformation of origin of current density (CTOCD).[36] Newer, more sophisticated techniques also include electron correlation effects, such as the multiconfiguration self-consistent-field method MCSCF,[15,53] the multiconfiguration MC-IGLO[56] approach, the coupled cluster CC[33] technique, the Møller−Plesset perturbation theories MP2-GIAO,[57] MP3-GIAO,[22] and MP4-GIAO,[24] and the second-order polarization propagator approximation (SOPPA), which was combined with LORG to second-order (LORG SOLO).[10] Recent reviews of these calculations can be found in refs 16 and 21.

For organic molecules of intermediate size such quantum chemical calculations have achieved only recently a sufficient level of accuracy for allowing a quantitative correlation with experimental data. In many cases only the isotropic part of the chemical shielding is evaluated, while for the full analysis all six tensor elements describing magnitude and orientation have to be considered (possible antisymmetric contributions of the CS tensor are neglected, since they do not contribute to the NMR frequencies[50]). Correspondingly, the experimental determination requires single-crystal measurements and their rotation pattern.

For the important case of carbon nuclei such a full set of data is available only in a few cases because of experimental difficulties. ^{13}C has only 1% natural abundance and a comparatively small gyromagnetic ratio, resulting in small signal amplitude; moreover, the spin-lattice relaxation time in compounds without mobile groups is slow and thus makes signal acquisition slow and tedious.

Such low detection sensitivity has been from the early days of solid state nuclear magnetic resonance one of its most severe limitations; on the other hand, this basic disadvantage stimulated active research on methods of sensitivity enhancement, which not only led to astounding signal-to-noise improvements but also gave deep insight in the physics of spin systems. Dynamic nuclear polarization (DNP) schemes[1,30,44] and double-resonance techniques employing direct or indirect detection[9,29,37] are prominent examples. The various double-resonance techniques obtain their sensitivity enhancement in two alternative ways. Optical detection of magnetic resonance (ODMR) increases sensitivity via a quantum transformation, i.e., the conversion of low energy rf quanta with small detection probability to optical quanta of higher energy and therefore higher detection probability. Proton enhancement[45−47] and DNP techniques, on

* E-mail: bunt@chemie.fu-berlin.de.
† Institut für Organische Chemie der Freie Universität Berlin.
‡ Institut für Experimentalphysik.
§ Institute of Physics, Silesian University.
|| Polish Academy of Sciences.
⊥ Institute of Chemistry, Silesian University.

S1089-5639(98)00718-X CCC: $15.00
Published on Web 06/29/1998

the other hand, increase sensitivity by increasing the sample magnetization by using an auxiliary reservoir of spins that can be polarized fast and effectively to generate spin order which in a following step is transferred to the spin system to be observed.

In the study presented here we use the technique of optical nuclear polarization (ONP) for efficient ^{13}C NMR sensitivity enhancement, allowing us to obtain full rotation patterns in three independent planes for all carbon positions in fluorene ($C_{13}H_{10}$).

Optical Nuclear Polarization

Optical nuclear polarization (ONP) is one version of the above-mentioned polarization-transfer methods. It makes use of the high electron spin polarization generated in the course of an optical pumping cycle. First experiments[40,41] on pure anthracene single crystals showed an increase of the proton polarization up to 3 orders of magnitude as compared to thermal polarization. Later investigations on several other molecular crystals (for example refs 7, 13, 32, 35, 43, 52, 54) showed that ONP is a rather common phenomenon in molecular crystals. In a typical ONP experiment, optically active molecules are photoexcited into a short-lived paramagnetic triplet state the polarization of which is used as source of spin order. In this way proton polarization levels of more than 40%[31] have been achieved. Further studies[2,4,12] showed that ONP works also with nonproton spins (^{13}C, ^{2}H).

ONP has several advantages, as compared to other dynamic polarization schemes:

(a) In general the excitation cycle is passed several times during a single experiment, because the cycle time is much shorter than the spin−lattice relaxation time of the nuclei determining the useful polarization time. This usually leads to accumulation of the polarization in the ground state, with the ONP active centers serving as polarization pumps.

(b) Polarization is created much faster by optical pumping than by thermal processes, which may require several hours in molecular crystals.

(c) The optically created triplet states, which are used in the ONP experiment, are short-lived. Therefore they do not influence the spectroscopy of the polarized nuclei.

(d) The electronic polarization is not limited by the Boltzmann factor; the optically created electronic polarization is usually much higher.

Despite this enormous gain in spin order, ONP has rarely been utilized for sensitivity enhancement in high-resolution solid-state NMR. A major reason lies in the fact that the efficiency of the ONP, i.e., the level of created polarization, depends strongly on the strength and direction of the external magnetic field. Optimum conditions for polarization are fields B_0 below 0.1 T with orientation of B_0 parallel to a fine structure principal axis of the involved triplet state. The sensitivity and resolution of the NMR detection, on the other hand, increases strongly with growing B_0 field.

To see how these factors affect the individual steps of the optical spin polarization cycle, the whole process is briefly summarized: The starting point is the singlet ground state S_0 of an optically active molecule in the external field B_p. Light irradiation leads to its excitation into a metastable triplet state T_1, usually via an intermediate excited singlet state. Due to selection rules governing the excitation and/or decay of T_1 (e.g., symmetry selection in the intersystem crossing), the three electronic spin sublevels exhibit different population numbers, corresponding to electronic spin order (OEP) in the triplet state.

By means of hyperfine coupling this order of electronic spins is partially transferred to neighboring nuclear spins. Particular transfer mechanisms are (a) mixing of state,[14] (b) cross relaxation with joint electronic and nuclear spin flips,[5] and (c) resonant irradiation of radio frequencies.[17,59] The short-lived T_1 state decays back into S_0, but this process does not affect the nuclear spin orientation. Thus, we obtain ground-state spin polarization. Spin diffusion leads to distribution of this localized polarization among the matrix nuclei. By repetitive execution of such optical pumping cycles nuclear polarization is accumulated. Finally, the magnetic field is set on resonance with the observation frequency and the pulse sequence for NMR detection is applied. Correspondingly, the main factors for achieving high polarization levels are (a) sufficient number of excitable molecules in contact with the nuclear spins of interest; (b) high photon flux for effective excitation plus high triplet yield with pronounced sublevel selectivity; (c) hyperfine interaction strong enough to transfer electronic polarization to nuclear spins in short times, before thermalization of the triplet spin order has occurred; (d) sufficiently fast triplet decay to avoid optical saturation; (e) efficient spin diffusion within the ground state; and (f) slow nuclear spin−lattice relaxation to allow exploitation of repetitive optical pumping cycles and to ensure conservation of spin order during the transfer to high field and until detection.

In principle, all of these factors depend on the particular nuclear spin species, e.g., on its abundance or its magnetic moment. In particular for localized triplet states insufficient ground-state spin diffusion can establish a serious bottleneck, because the nuclear polarization is created only at ONP active sites. In the case of low concentration of guest molecules, the situation can arise that soon all ONP active sites are highly polarized while the bulk of the matrix will get only low polarization. This case has for example been found in investigations of ^{2}H ONP of fluorene doped with acridine.[4] ^{13}C at natural abundance is another example of inefficient spin diffusion, because of its small gyromagnetic ratio, low abundance, and wide spectral range. However in this case the bottleneck can be effectively circumvented by using an indirect approach. The reservoir of ^{1}H spins with its efficient spin diffusion is used as an intermediate storage for the ONP created at the polarization field, and in a second step after switching to the detection field B_0 conventional $^{1}H-^{13}C$ cross-polarization is applied for enhancing the ^{13}C signal.

Experimental Section

Spectrometer. A description of our ONP spectrometer for proton polarization is given in ref 3. By means of a precision probe transfer the sample can be polarized between 0 and 0.1 T and the observation performed at 7.04 T. The present experiments are performed using an improved setup, which we shall describe briefly here.

The main experimental problem which rules out field-switching solutions by electric current control is due to opposing requirements concerning the external magnetic field for polarization and observation. For polarization, the highest efficiency is expected for fields typically well below $B_P = 0.1$ T, while for good detection sensitivity and spectral resolution observation fields B_0 above 4 T are desirable, in particular for nuclei with a low gyromagnetic ratio such as ^{13}C.

For our ONP experiment we use a mechanic field-cycling technique (see timing scheme, Figure 1) with two magnets in a tandem configuration with a common field axis along which the NMR probe is shuttled in a guiding cylinder.[6] One magnet

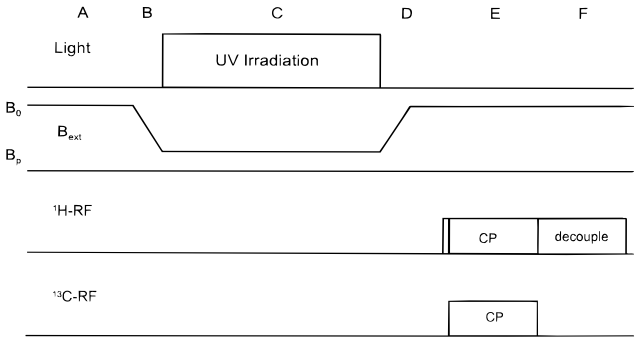

Figure 1. Timing scheme of the ONP-enhanced ^{13}C NMR experiment.

is a commercial cryomagnet with a field of $B_0 = 7.04$ T for the NMR detection; the other one, used for the polarization field B_P, is constructed as a pair of Helmholtz coils. The actual polarization field is a superposition of the field of the Helmholtz coils and the fringe field (about 52.4 mT at the sample position) of the superconducting magnet. B_P can be varied between 0 and 160 mT by use of a Hall control circuit. To avoid distortions of the detection field, the polarization magnet is switched off during signal acquisition.

For all measurements a specially designed NMR probe is used with windows for light irradiation and a precise crystal goniometer, which defines the coordinate system for sample rotation (x_{GON}, y_{GON}, z_{GON}). The sample is glued to a small quartz glass rod which is fixed inside a cog wheel. To allow different sample orientations for observation and polarization, the whole probe including the goniometer is pneumatically moved in the guiding cylinder. The transport time is around 3 s. During the transport, the orientation of the sample is automatically changed from the polarization position to the detection position. The efficiency of the ONP process depends strongly on the strength and direction of the polarization field B_p. All measurements in the *ab*-plane are performed by polarizing the protons at a field of $B_p = 8.5$ mT parallel to the *y*-axis of the radical pair fine structure tensor which lies in the *ab*-plane 10.5° away from the *a*-axis. The measurements in the *ac*- and *xz*-plane are performed by polarizing the protons at a field of $B_p = 8.0$ mT oriented along the *x*-axis of the radical pair fine structure tensor which coincides with the crystal *c*-axis. For exact timing, the whole ONP cycle is computer controlled using a VME bus system. A more detailed description of the apparatus will be given elsewhere.

NMR detection is performed at a ^{13}C Larmor frequency of 75 MHz, employing a commercial spectrometer connected to a UNIX workstation for data analysis. The ^{13}C spectra were calibrated with respect to TMS by using the well-known ^{13}C positions of adamantane as an intermediate standard. The typical 90° pulse width is about 1.8 μs both for protons and carbons, and the optimized contact time for the ^1H ^{13}C cross-polarization is 3 ms. The spectral resolution, measured via the line width after shimming (spherical water sample), is 0.1 ppm. For light irradiation a 100 W Hg lamp is used in combination with an IR and a 370 nm UV cutoff filter to minimize thermal deterioration of the crystal. The typical irradiation time was 30 s.

Samples and Preparation. The fluorene material used for our experiments was synthesized and highly purified by extensive zone refining The nominal doping concentration in the melt was 1000 ppm of acridine. Single crystals were grown by the Bridgman technique. Out of a single crystal a cube of approximately 4 mm length was cut, oriented by use of an optical two-circle goniometer and a polarizing microscope, and

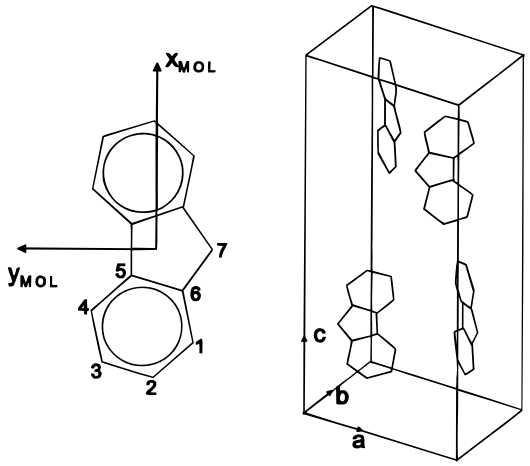

Figure 2. Fluorene molecule and unit cell of the fluorene single crystal and definition of molecular and crystal axis system.

finally glued onto the top of a quartz glass sample holder. The accuracy achieved by this orientation method was better than 2°. The exact orientation of the sample was determined by the angular dependence of the NMR transition frequencies.

In the literature, there exist several slightly different crystal structures of fluorene. Either a planar configuration of the carbons was found,[8,11] which corresponds to molecular C_{2v} symmetry, or a slightly bent arrangement (0.77° angle between aromatic planes at room temperature) was measured,[26] which corresponds to molecular C_s symmetry. Except for these differences, the two newer X-ray investigations[8,26] accord in the following results: The orthorhombic fluorene unit cell (Figure 2) contains four molecules in two magnetically inequivalent positions.

In the case of C_{2v} symmetry there is a unique choice of the molecular axis system: the axis corresponding to the C_2 rotation, y_{MOL}, and the normal vectors of the two σ_v mirror planes, x_{MOL} and z_{MOL}. In the case of the C_s symmetry the only special axis is the normal vector of the σ_h mirror plane, and there is an ambiguity in the choice of the two remaining axes. Therefore the following definition of the molecular axis system, which is equivalent to the C_{2v} case, is used: The molecular *x*-axis, x_{MOL}, is the normal of the mirror plane σ_h, the molecular *y*-axis, y_{MOL}, is the line defined by the carbons C7 and the middle of the line from carbon C4 to carbon C4′, and the molecular *z*-axis is the normal of the plane defined by x_{MOL} and y_{MOL}. For simplicity, in the following the plane spanned by the molecular x_{MOL} and y_{MOL} axes is called the molecular plane. When assuming C_{2v} symmetry of the molecule, this plane is identical to the aromatic carbon plane. The x_{MOL} axis is identical with the crystal *c*-axis.

For the planar configuration[8] the angle between the crystal *b*-axis and the molecular *y*-axis y_{MOL} is 34.4°. For the bent configuration[26] the angle between the y_{MOL} and the crystal *b*-axis is 33.9°. The long axes of all molecules are perpendicular to the crystallographic *ab*-plane.

For light irradiation a mercury lamp was used, allowing effective excitation of the acridine singlet S_2 state with subsequent intersystem crossing to the lowest triplet T_1 state. T_1 is a precursor of an efficient intermolecular hydrogen transfer reaction leading to the formation of a fluorenyl−acridinyl radical pair in its triplet state.[23,39] The ONP discussed here results from electronic spin order of this localized radical pair triplet state. Its zero-field splitting tensor has two of its principal axes in the crystallographic *ab*-plane; therefore, all experiments are performed with the B_p field vector in this plane.

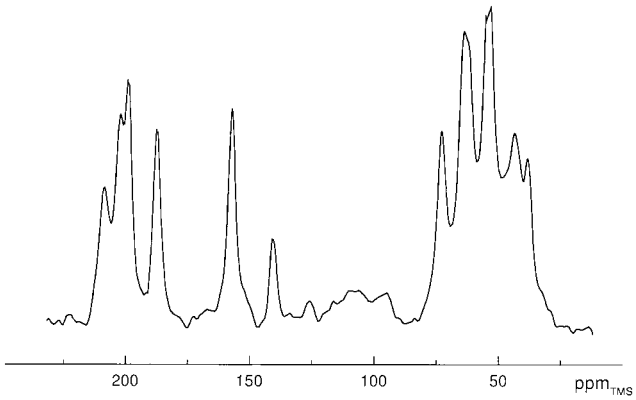

Figure 3. Typical ^{13}C CP spectrum after optical nuclear polarization of the protons. The spectrum was obtained in the crystal *ab*-plane at an angle of $-105°$ with respect to the crystal *a*-direction.

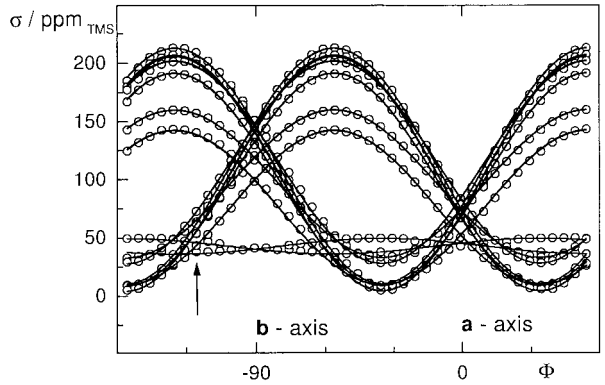

Figure 4. Rotation pattern in the crystal *ab*-plane ($a = 0°$). The arrow marks the angle where the spectrum shown in Figure 3 was measured.

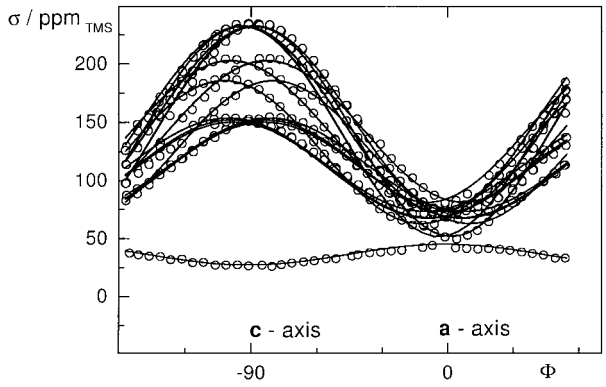

Figure 5. Rotation pattern in the crystal *ac*-plane ($a = 0°$).

Data Evaluation. The angular dependence of the NMR transition frequencies was measured in the *ab* and *ac* crystal planes and in the molecular xz_{MOL} plane. All line positions were plotted as a function of the orientation of the detection field (rotation patterns, Figures 4−6). In a first step the individual NMR transitions (line positions) at the different orientations were combined to sets of angular dependences. After assigning all spectral lines, the parameters of eq 5 were calculated for all lines. In this way all three rotation patterns were evaluated. By comparing the resonance frequencies at the intersection axes of the experimental planes, the parameters obtained from the different planes could be assigned with respect to each other. For each individual set of lines the CS tensor in the crystal axis system was determined from these elements, and the principal values and directions of the shielding interaction were calculated by numerical diagonalization of their tensors. To account for imperfections in the orientation of the crystals, the resulting tensors were used to calculate all three rotation patterns and the relative orientations of the three planes were optimized. The final error in the relative orientations was less than 0.5°.

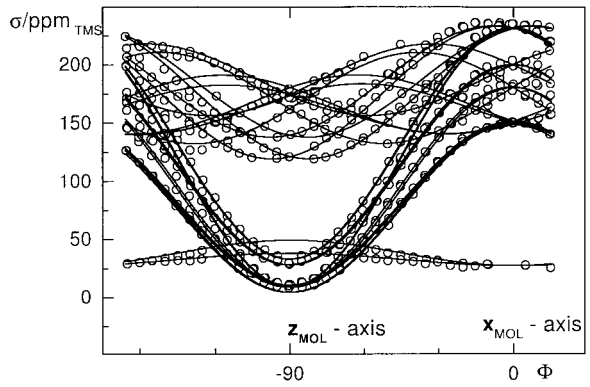

Figure 6. Rotation pattern in the molecular xz_{MOL}-plane ($x_{MOL} = 0°$).

Chemical Shift Calculations. Fluorene ($C_{13}H_{10}$) is a rather large molecule for ab initio calculations. To allow a treatment of this system with reasonable effort, the ab initio calculations were performed using some of the less sophisticated calculation approaches and reference calculations of similar systems were used to account for the errors caused by the models.

Because of the differences in the molecular structures found by X-ray diffraction, a calculated molecular structure was chosen as a starting point of the ab initio calculations of the CS shielding tensors. All calculations were performed for the gas phase of the molecule.

The chemical shift calculations were performed in the following way: For the density functional (DFT) calculations of the ^{13}C shielding parameters a fully optimized geometry of the fluorene molecule was used by employing the MM+ Molecular Modeling method (HYPERCHEM 4.5) followed by a single-point GIAO NMR[60] calculation using Gaussian 94 software.[38] We selected three different basis sets for the geometry optimization using the DFT[51] method: 6-31G* (small), 6-31+G* (medium), and 6-311++G** (large). At all levels of theory a planar ring arrangement of the fluorene molecule is predicted. For all GIAO NMR calculations the standard notation for the basis set and geometry optimization was used, for example DFT-B3PW91/6-311+G*//DFT-B3PW91/6-31+G*. For calibrating our calculations against the usual TMS standard the known geometry of methane and benzene molecules was optimized using the same methods. Their isotropic chemical shift was used (benzene for the aromatic parts and methane for the methylene bridge) to adapt the calculated fluorene tensors to the experimental results.

Theoretical Section

The mechanism of proton ONP in the fluorene/acridine system is well understood, and in the present context the ONP is used only as a spectroscopic tool for sensitivity enhancement. Therefore no theoretical description of the ONP process is given here. For a detailed description of the proton ONP phenomenon itself the reader is referred to ref 54.

In the present work single-crystal studies of natural-abundance ^{13}C NMR are performed. Due to the low ^{13}C concentration, any homonuclear $^{13}C-^{13}C$ interaction can be neglected. Under conditions of proton decoupling, the ^{13}C rotating frame spin Hamiltonian consists simply of the chemical shift term, which can be described by the chemical shielding tensor $\vec{\sigma}$ represented by a real, symmetric 3×3 matrix:

$$\hat{H} = \gamma_I \vec{B}_0 (1 - \vec{\sigma}_I)\hat{\mathbf{I}} \tag{1}$$

At high magnetic field B_0, only the secular part of the interaction is effective. If B_0 points along the *z*-direction, one obtains

$$\hat{H} = \gamma_I B_0 (1 - \sigma_{Izz})\hat{I}_z \tag{2}$$

The secular component σ_{zz} of the chemical shielding tensor depends on the relative orientation of B_0 with respect to the internal molecular coordinate system. If $\vec{b}$ is a unit vector pointing into the direction of the magnetic field,

$$\vec{b} = \vec{B}_0/B_0 \tag{3}$$

the tensor element σ_{zz} is given as

$$\sigma_{zz} = \vec{b}\vec{\sigma}\vec{b} \tag{4}$$

A detailed description of the evaluation of orientation-dependent NMR experiments on single crystals (rotation pattern) can be found in ref 42. Here only some salient features are reproduced. A rotation of the molecule, with respect to the single crystal, in the goniometer around an axis, which is not parallel to $\vec{b}$, will lead to an orientation dependence of σ_{zz}. In particular if the rotation axis is chosen as the y_{GON}-axis perpendicular to the magnetic field, one obtains

$$\sigma_{zz}(\varphi) = \frac{\sigma_{11} + \sigma_{33}}{2} + \frac{\sigma_{11} - \sigma_{33}}{2}\cos(2\varphi) + \frac{\sigma_{13} + \sigma_{31}}{2}\sin(2\varphi) \tag{5}$$

Thus by rotating the sample in the xz_{GON}-plane, it is possible to determine the tensor elements (σ_{11}, σ_{31}, σ_{13}, and σ_{33}) in the laboratory frame, which, however, depend on the particular orientation of the crystal in the goniometer. If several crystal planes with known relative orientations are chosen, all elements of the tensor can be determined, and from these elements the whole tensor in the crystal frame can be constructed. Diagonalization of this tensor or, more generally, when several inequivalent carbon positions are present in the molecule, of all these tensors, gives the principal elements and directions of the shielding tensors in the crystal frame, which are related to the molecular geometry.

Results and Discussion

Experimental Results. Before analyzing the angular dependence of the NMR transition frequencies in detail, some general features of the results, which are evident from the molecular and crystal structure of fluorene, will be discussed (see Figure 2). There are two magnetically inequivalent fluorene positions in the unit cell and 13 carbon atoms in each fluorene molecule. Six of these carbon atoms are located in each of the two benzene rings, and the last carbon is in the methylene group (C7) between the rings. In the most general case, the fluorene ^{13}C spectrum will consist of 26 distinct lines. In the planes of symmetry of the crystal, lines of symmetry equivalent carbons (with respect to the plane) will coincide, leading to a reduction of the number of lines. The crystal symmetry is also reflected in the angular dependence of the resonance frequencies in the crystallographic *ab*- and *ac*-planes, because the rotation patterns are symmetric with respect to the crystal axes. This can be used as a guideline for the assignment of the angular dependence to one of the two inequivalent molecular orientations or one of the two aromatic rings. Another type of symmetry, which can be exploited for the assignment, is the molecular symmetry of the fluorene molecule. In the case of the planar gas-phase configuration of the fluorene molecule, the molecular *z*-axis is a principal axis of all ^{13}C tensors in the molecule. In principle this molecular symmetry can be broken in the crystal, due to intermolecular interactions, crystal packing effects, or asymmetric motion of the molecule. Assuming that these effects can be neglected in the fluorene crystal, it follows that for a planar configuration of fluorene the molecular *z*-axis is still a principal axis of all ^{13}C tensors.

Figure 3 shows a typical experimental ^{13}C NMR spectrum after ONP and subsequent multiple contact cross-polarization from the protons to the ^{13}C nuclei (four contacts). Sixteen acquisitions are accumulated. With an optical pumping time of 30 s and a field cycling time of 3 s the time for each scan is around 40 s; accordingly the total time for obtaining one spectrum is less than 15 min. This allows one to measure rotation patterns in steps of 5°. Considering the estimated gain in sensitivity by a factor of around 100 with respect to thermal polarization of the proton reservoir, it becomes clear that with standard techniques such studies are hardly feasible.

Several lines from inequivalent ^{13}C positions are clearly resolved, and their spectral positions can be determined with an accuracy of 0.2 ppm. Spectra of this kind have been measured in the crystal *ab*- and *ac*-planes and in the molecular xz_{MOL}-plane, and the resulting line positions have been plotted as a function of the orientation of the detection field (rotation patterns).

***B*$_0$ in the *ab*-Plane.** Depending on the symmetry of the fluorene molecule in the crystal the crystallographic *ab*-plane is either a molecular σ_v (C_{2v} symmetry) or σ_h (C_s symmetry) mirror plane of the fluorene molecule. For both possible symmetries the two aromatic rings of the molecule are rendered magnetically equivalent. Thus 14 lines, seven for each fluorene molecule, are expected at maximum: six from the aromatic carbons and one from the methylene group (C7). The resulting rotation pattern is shown in Figure 4. The open circles mark the experimental line positions, and the solid lines are the calculated line positions using the results from a tensor fit. The pattern can be roughly subdivided into three sets of lines: one set of two lines varying in the range between 30 and 50 ppm and two sets of lines varying in the range between 10 and 220 ppm, all of which have their minimum at −34° and +34°, respectively. Since the latter two sets are mirror symmetric with respect to the crystal axes, it is evident that these two sets of lines have to be attributed to the two magnetically inequivalent fluorene molecules. From the range of CS values of these lines, it is evident that these lines have to be attributed to the aromatic carbon positions. The remaining two lines between 30 and 50 ppm are assigned to the methylene groups (C7) of the two magnetically inequivalent fluorene molecules.

***B*$_0$ in the *ac*-Plane.** The crystallographic *ac*-plane is a crystal mirror plane for the two magnetically inequivalent fluorene molecules, rendering all molecules in the unit cell equivalent. Thus for an arbitrary orientation in this plane, 13 lines are expected: two times six from the aromatic carbons and one from the methylene group. The resulting rotation pattern is shown in Figure 5. The open circles mark again the experimental line positions, and the solid lines are the calculated line positions, using the results from the tensor fit. There are two sets of lines visible in the rotation pattern: one set with CS values in the range from 50 to 240 ppm and one set of lines (including only a single line) at 50 ppm. Employing the same argumentation as above, the single line can be attributed to the C7 position and the remaining 12 lines to the aromatic carbon positions.

TABLE 1: Effect of Basis Set and Geometry on DFT-B3PW91 Calculated ^{13}C Fluorene Shielding

A: Isotropic Shielding [ppm]

atom no.	B3PW91/ 6-31G*//6-31G*	B3PW91/ 6-31+G*//6-31+G*	B3PW91/ 6-311+G*//6-31+G*	B3PW91/ 6-311++G**//6-311++G**	B3PW91/ 6-311++G**//MM+	RHF/ 6-311++G**//MM+
C1	73.77	73.59	57.06	57.07	51.73	56.57
C2	72.19	72.00	55.42	55.28	53.98	59.40
C3	71.71	71.49	55.12	55.07	52.54	57.85
C4	78.11	78.41	62.11	62.17	62.00	66.98
C5	56.70	55.52	38.68	39.01	44.43	50.15
C6	55.17	54.16	36.83	37.21	34.54	40.76
C7	156.00	155.87	145.81	145.75	145.51	159.08

B: Shielding Anisotropy [ppm]

atom no.	B3PW91/ 6-31G*//6-31G*	B3PW91/ 6-31+G*//6-31+G*	B3PW91/ 6-311+G*//6-31+G*	B3PW91/ 6-311+G*//6-311++G**	B3PW91/ 6-311++G**//MM+	RHF/ 6-311++G**//MM+
C1	156.42	155.55	171.22	171.30	170.75	181.21
C2	162.60	161.55	177.94	178.61	173.82	183.02
C3	164.03	163.78	180.87	181.55	180.22	188.29
C4	158.15	157.26	171.91	172.58	168.73	177.06
C5	150.24	150.97	162.29	162.72	165.60	178.31
C6	158.71	160.16	172.29	173.13	165.82	179.94
C7	28.80	29.41	31.75	31.46	24.84	23.06

***B*$_0$ in the *xz*-Plane.** In principle, the results from the *ab*- and *ac*-planes are already sufficient to determine the ^{13}C CSA tensors. However, none of these planes coincide with a plane where the principal values of the tensors are expected, due to the molecular symmetry of the fluorene molecule. Therefore, additional measurements in the molecular xz_{MOL}-plane were performed. There is no direct symmetry relationship between the lines of this molecule and the lines from the second, inequivalent molecule. The resulting rotation pattern is shown in Figure 6. Three different sets of lines are visible: one set with two lines in the range from 30 to 50 ppm, which can be attributed to two, inequivalent methylene (C7) positions, one set of lines in the range from 10 to 230 ppm, which, because of their higher anisotropy, can be attributed to the aromatic carbon positions of the first molecule, corresponding to the xz_{MOL}-plane, and one set of lines in the range from 130 to 230 ppm, which can be attributed to the aromatic carbon positions of the second molecule. The latter two sets of lines intersect at the crystal *c*-axis ($\Phi = 0°$). Since the molecular x_{MOL}-axis of all molecules coincides with the crystal *c*-axis, this angle is used to determine the orientation of the molecular x_{MOL}-axis.

Assignment of Tensors to Molecular Positions. In a next step the different ^{13}C tensors were determined from the rotation patterns. It was evident from the symmetry of the rotation patterns which tensors belong to symmetry-related molecular positions. The assignment of these tensors to individual molecular positions was done in the following way:

(1) Compare the trace of the ^{13}C CSA tensor to the isotropic value from ^{13}C solution NMR.

(2) Compare the principal axes directions to directions of bond directions.

(3) Compare symmetry-related tensors.

(4) Compare the PAS directions of the experimental tensors to the PAS directions of calculated tensors (see below).

With the exception of the molecular positions 5 and 6, all tensors could be assigned employing the first three strategies, because the isotropic CS and the direction of the −CH bond allowed an unambiguous assignment. For the positions 5 and 6 however, the isotropic CS values nearly coincide and additional information from the calculations was needed. The result is displayed in Table 3, which shows the experimental CS tensors and the orientation of these tensors in the molecular plane.

Results from ab Initio Calculations. In a first step DFT calculations (also SP GIAO RHF at MM+ and semiempirical PM3 optimized geometry) were performed for methane and benzene as reference compounds for basis sets of different complexity (results not shown). The calculated structural parameters for the reference compounds were in good agreement with the experimental data from all applied methods. In a second step the isotropic shielding parameters were calculated for these geometries. The results depend strongly on the basis set (methane 12 ppm, benzene 34 ppm difference between calculations with small basis sets 3-21G and calculations with large basis sets 6-311++G**) and on the starting geometry (typically 5 ppm) used in the shielding calculations. In the same way the structural parameters of the fluorene molecule in the gas-phase approximation for different basis sets and geometries were calculated. The DFT-predicted C−C bonds are in good agreement with the planar experimental crystal structure (X-ray data) of ref 8. Typical deviations between experimental and calculated C−C bond lengths are 0.005−0.01 Å. The MM+ method gives similar results, with the exception of the C5−C5′ bond, which is strongly underestimated by about 0.07 Å. All calculated C−H bonds are close to the standard values of about 1.09 Å for both DFT and MM+ optimization. The differences between experimental and calculated C−H bond length can be attributed to the well-known difficulties of locating hydrogen atoms by X-ray diffraction.

Table 1 shows the results of a single-point GIAO CS calculation on fluorene using the DFT method. The isotropic shieldings and the anisotropy parameters are more influenced by the chosen basis set than by the chosen geometry. The small basis set calculation predicts too large isotropic shielding values. Parallel to the enlarging of the basis sets, the calculated isotropic shieldings decrease. There is a large gap (17 ppm) between the isotropic shielding of ring carbon atoms, calculated with the 6-31G* and 6-31+G* basis sets using DFT geometries at the same level, with the results obtained with larger basis sets (DFT/6-311++G**). For these larger sets, there are only small differences caused by the applied geometry. Comparing these calculated values with the experimental shielding data, it is evident that the DFT predicts higher values of the fluorene ^{13}C shielding anisotropy than found in our experiment. Typical deviations between experimental and calculated values are in the range 10−30 ppm (see Table 1).

TABLE 2: Comparison of Calculated and Experimental CS Tensors after Adjusting the Trace of the Calculated Tensors

chemical shift components $\sigma(ii)$ [ppm]	atom no. [11]	σ_{ii} exptl	DFT/ 6-31G*// 6-31G*	DFT/ 6-31+G*// 6-31+G*	DFT/ 6-311+G*// 6-31+G*	DFT/ 6-311++G**// 6-311++G**	DFT/ 6-311++G** //MM+	RHF/ 6-311++G** //MM+
$\sigma(xx)$	C1	220.9	214.6	215.9	227.3	226.7	233.4	244.0
$\sigma(xx)$	C2	235.7	221.5	222.9	234.9	234.7	232.5	241.6
$\sigma(xx)$	C3	230.4	222.2	224.1	236.1	235.7	235.6	244.6
$\sigma(xx)$	C4	211.7	209.1	209.3	219.5	219.1	217.9	227.1
$\sigma(xx)$	C5	234.9	226.0	227.6	235.1	235.0	223.2	234.2
$\sigma(xx)$	C6	231.9	225.1	226.3	234.9	234.8	235.5	246.7
$\sigma(xx)$	C7	48.9	60.3	60.7	55.4	55.3	44.6	36.7
$\sigma(yy)$	C1	142.9	141.1	137.9	137.3	138.0	138.2	135.1
$\sigma(yy)$	C2	138.2	141.5	138.0	137.5	138.5	136.6	133.1
$\sigma(yy)$	C3	141.8	142.8	139.3	138.9	139.7	140.7	136.6
$\sigma(yy)$	C4	143.8	139.1	135.9	135.5	136.2	131.8	128.3
$\sigma(yy)$	C5	157.0	159.8	159.2	160.1	160.0	159.5	155.8
$\sigma(yy)$	C6	170.4	169.4	169.4	170.9	170.8	167.1	163.2
$\sigma(yy)$	C7	36.6	45.9	44.3	38.8	38.8	44.2	31.9
$\sigma(zz)$	C1	10.5	21.4	21.3	11.1	11.0	15.0	8.3
$\sigma(zz)$	C2	10.0	18.9	18.9	8.3	7.9	10.7	4.3
$\sigma(zz)$	C3	9.6	18.4	17.9	6.6	6.2	7.9	2.3
$\sigma(zz)$	C4	5.3	16.0	15.3	5.6	5.0	6.1	0.7
$\sigma(zz)$	C5	33.4	42.6	42.4	35.6	34.8	25.8	16.7
$\sigma(zz)$	C6	28.6	38.5	37.7	30.6	29.7	35.5	25.0
$\sigma(zz)$	C7	27.4	24.3	23.1	15.3	15.6	18.5	11.2

TABLE 3: Principal Values of Experimental Tensors [ppm], Anisotropy Δ [ppm], Asymmetry Parameter η, and Experimental and Calculated Tensor Orientation (in deg)

atom no.	$\sigma(xx)$	$\sigma(yy)$	$\sigma(zz)$	σ(iso)	$\lvert\Delta\rvert$	$\lvert\eta\rvert$	ϕ exptl	ϕ calc
C1	221	143	11	125	114	0.68	71.8	71.7
C2	235	138	10	128	118	0.82	9.8	10.8
C3	230	142	9	127	118	0.75	−48.5	−48.6
C4	211	143	5	120	115	0.59	−107.0	−105.1
C5	235	157	33	142	109	0.72	−45.7	−43.2
C6	232	170	28	143	115	0.54	10.2	7.0
C7	27	37	49	38	11	0.91	1.1	0.0

A strong improvement of the calculated shielding parameters is obtained if the calculated tensor eigenvalues are shifted in the following way: reference calculations of benzene (for the aromatic carbons) and methane (for the methylene carbon) are performed on the same theoretical level and the deviation between experimental and calculated isotropic chemical shifts is determined. These values are used for modifying the fluorene calculations. The result after such a shifting is shown in Table 2. In this case, there is a rather good agreement between calculated and experimental shielding tensors. Such an agreement is found for all levels of calculation, i.e., the larger deviations of the smaller basis sets are canceled by the equivalent deviations from the reference calculation.

Discussion

Unlike for systems with excitonic triplet states, where direct polarization of ^{13}C carbons is very efficient,[2,4] in fluorene crystals with the triplets localized near the acridine guest molecules the indirect polarization via the ^{1}H reservoir is far superior. In this way the NMR signal aquisition time can be kept so short that rotation patterns with good signal/noise can be measured with high angular resolution in a redundant number of planes. The experimental accuracy allows the determination of the tensor eigenvalues with an accuracy of ± 0.5 ppm and of orientations in the molecular and the crystal coordinate frame within $\pm 0.5°$.

As an experimental example the ^{13}C solid-state NMR spectra of fluorene single crystals after optical nuclear polarization have been recorded in the *ab*, *ac*-, and xz_{MOL} crystal planes. From the rotation patterns the ^{13}C chemical shielding tensors of all 13 fluorene carbon atoms have been determined. The orientations of these tensors in the molecular coordinate system of the fluorene as well as in the crystal coordinate system of the fluorene single crystal have been determined from the experimental data with very high precision (0.5°). The principal values of the aromatic ^{13}C chemical shielding tensors corroborate previous results obtained at similar systems[19] and exhibit the typical strong shielding anisotropy of aromatic carbon atoms. The principal axes systems of these tensors were found to be closely linked to the molecular coordinate system of the fluorene molecule. In particular all tensors have one principal axis in common, which corroborates the planar nature of the fluorene molecule (within 0.4°), as was suggested by X-ray work[8] and our own results from ^{2}H NMR measurements on fluorene single crystals.[4,12] This common *z*-axis is perpendicular to the molecular plane. For the aromatic carbon atoms with a −CH bond (carbon positions C1, C2, C3, and C4) the principal axis corresponding to the largest principal value is in the direction of this −CH bond. For the remaining aromatic carbon positions (C5, C6) the direction corresponding to the largest principal value is close (within 4°) to the C4−C5 bond direction for the C5 carbon and close (within 4°) to the C1−C6 bond direction for the C6 carbon. The ^{13}C chemical shielding of the methylene carbon (C7) exhibits the typical small anisotropy of an sp^3-hybridized carbon.[20,58] Due to this small anisotropy, the determination of the principal axis system in the molecular coordinate system is less accurate than for the aromatic carbon atoms. From the molecular symmetry (planarity and molecular *y*-axis being a C_2 axis) it is evident that the principal axes of this tensor are parallel to the molecular axes of the fluorene molecule. The angle between the *z*-axes of the ^{13}C chemical shielding tensors and the crystal *b*-axis is $(34.2 \pm 0.5)°$, which can be interpreted as being half the angle between the molecular planes of the two inequivalent positions. This angle agrees closely with the angle found from our ^{2}H NMR measurements and with the value found from X-ray diffraction.[8,26]

The experimental tensor values are compared to calculated tensor values from ab initio calculations employing single-point GIAO NMR calculations. The calculated tensor eigenvalues depend strongly on the chosen method, in particular on the selected basis set. They are also, however to a smaller extent, influenced by the assumed geometry of the molecule. The

calculated isotropic shielding values exhibit systematic deviations from the experimental shielding. The calculated shielding anisotropies are in a good agreement with the experimental values, and the calculated PAS directions agree excellently with the experimentally found PAS.

The accuracy of the isotropic shielding calculations can be significantly improved by adjusting the trace of the calculated tensor employing results from reference calculations of benzene and methane, respectively. This gives a good agreement (within 10% of the size of the CS anisotropy) between calculated and experimental ^{13}C chemical shielding tensor values on all levels of sophistication. On this level the accuracy of calculated CS parameters of larger molecules is thus found comparable to the accuracy of small reference molecules, and the remaining deviation, in particular for the more sophisticated basis sets, might originate in crystal effects, which are not included in the gas-phase calculations.

Summary and Conclusion

In summary, it has been shown that the combination of optical nuclear polarization with standard cross-polarization techniques allows detailed NMR spectroscopic studies in solid-state systems with very unfavorable relaxation parameters. Applying this method to monocrystalline fluorene doped with nominally 1000 ppm acridine, it was possible to determine the ^{13}C chemical shielding tensors of all fluorene carbon position atoms and verify the planar molecular structure of the fluorene molecule ground state in the single crystal within 0.4°, which is comparable to the accuracy obtainable from X-ray studies.

Acknowledgment. Financial support by the Deutsche Forschungsgemeinschaft (Sfb 337) is gratefully acknowledged.

References and Notes

(1) Abragam, A.; Proctor, W. G. *C. R. Acad. Sci. Paris* **1958**, *246*, 2253.
(2) Allgeier, J. Ph.D. Thesis, FU Berlin, 1987.
(3) Allgeier, J.; Buntkowsky, G.; Hentrich, S.; Nack, M.; Vieth, H. M. *Ber. Bunsen-Ges. Phys. Chem.* **1989**, *93*, 1281.
(4) Allgeier, J.; Buntkowsky, G.; Hentrich, S.; Hoffmann, W.; Vieth, H. M. *Isr. J. Chem.* **1993**, *32*, 205.
(5) Allgeier, J.; Macho, V.; Stehlik, D.; Vieth, H. M.; Auch, W.; von Schuetz, J. U. *Chem. Phys. Lett.* **1982**, *86*, 522.
(6) Allgeier, J.; Vieth, H. M. In *Proceedings of the 23th Congress Ampere Rome*; Istituto Superiore di Sanitá: Roma, Italy, 1986; p 578.
(7) Auch, W.; von Schuetz, J. U. *Phys. Status Solidi b* **1980**, *101*, 287.
(8) Belsky, V. K.; Zavodnik, V. E.; Vozzhennikov, V. M. *Acta Crystallogr.* **1984**, *C40*, 1210.
(9) Bleich, H. E.; Redfield, A. *J. Chem. Phys.* **1971**, *55*, 5406.
(10) Bouman, T. D.; Hansen, A. E. *Chem. Phys. Lett.* **1990**, *175*, 292.
(11) Brown, G. M.; Bortner, M. H. *Acta Crystallogr.* **1954**, *7*, 139.
(12) Buntkowsky, G. Ph.D. Thesis, FU Berlin, 1991.
(13) Buntkowsky, G.; Nack, M.; Stehlik, D.; Vieth, H. M. *Isr. J. Chem.* **1989**, *29*, 109.
(14) Colpa, J. P.; Stehlik, D. *Chem. Phys.* **1977**, *21*, 273.
(15) Dalgaard, E.; Jorgensen, P. *J. Chem. Phys.* **1978**, *69*, 3833.
(16) de Dios, A. C. *Progr. NMR Spectrosc.* **1996**, *29*, 229.
(17) Deimling, M.; Brunner, H.; Dinse, K. P.; Hausser, K. H.; Colpa, J. P. *J. Magn. Reson.* **1980**, *39*, 145.
(18) Ditchfield, R. *J. Chem. Phys.* **1972**, *56*, 5688.
(19) Duncan, T. M. *A Compilation of Chemical Shift Anisotropies*; The Farragut Press: Chicago, 1990.
(20) Facelli, J.; Grant, D. M.; Michl, J. *Acc. Chem. Res.* **1987**, *20*, 152.
(21) Fukui, H. *Progr. NMR Spectrosc.* **1997**, *31*, 317.
(22) Fukui, H.; Baba, T.; Matsuda, H.; Miura, K. *J. Chem. Phys.* **1994**, *100*, 6608.
(23) Furrer, R.; Heinrich, M.; Stehlik, D.; Zimmermann, H. *Chem. Phys.* **1979**, *36*, 27.
(24) Gauss, J. *Chem. Phys. Lett.* **1994**, *229*, 198.
(25) Geertsen, J. *Chem. Phys. Lett.* **1991**, 479.
(26) Gerkin, R.; Lundstedt, A.; Reppart, W. *Acta Crystallogr.* **1984**, *C40*, 1892.
(27) Hameka, H. F. *Mol. Phys.* **1958**, 203.
(28) Hansen, A. E.; Bouman, T. D. *J. Chem. Phys.* **1985**, *82*, 5035.
(29) Hartmann, S. R.; Hahn, E. L. *Phys. Rev.* **1962**, *128*, 2042.
(30) Hausser, K. H.; Stehlik, D. *Adv. Magn. Reson.* **1968**, *3*, 79.
(31) Kesteren, H. W. v.; Wenckebach, W. T.; Schmidt, J. *Phys. Rev. Lett.* **1985**, *55*, 1642.
(32) Kolb, H.; Wolf, H. C. *Z. Naturforsch.* **1972**, *27a*, 51.
(33) Kutzelnigg, W. *Modern Theoretical Chemistry*; Plenum: New York, 1977; Vol. IIIA.
(34) Kutzelnigg, W. *Isr. J. Chem.* **1980**, *19*, 193.
(35) Lau, P.; Stehlik, D.; Hausser, K. H. *J. Magn. Reson.* **1974**, *15*, 270.
(36) Lazaretti, P.; Malagoli, M.; Zanasi, R. *Chem. Phys. Lett.* **1994**, *220*, 299.
(37) Lurie, F. M.; Slichter, C. P. *Phys. Rev.* **1964**, *133a*, 1108.
(38) Frisch, M. J.; et al. *Gaussian 94, Revision C.3*; Gaussian Inc.: Pittsburgh, PA, 1995.
(39) Macho, V.; Colpa, J. P.; Stehlik, D. *Chem. Phys.* **1979**, *44*, 113.
(40) Maier, G.; Haeberlen, U.; Wolf, H. C. *Phys. Lett.* **1967**, *25a*, 323.
(41) Maier, G.; Haeberlen, U.; Wolf, H. C.; Hausser, K. H. *Phys. Lett.* **1967**, *25a*, 384.
(42) Mehring, M. *High-Resolution NMR Spectroscopy in Solids*; Springer-Verlag: Berlin, 1983.
(43) Oshiro, C. Ph.D. Thesis, UC Berkeley, 1982.
(44) Overhauser, A. W. *Phys. Rev.* **1953**, *92*, 411.
(45) Pines, A.; Gibby, M. G.; Waugh, J. *J. Chem. Phys.* **1972**, *56*, 1776.
(46) Pines, A.; Gibby, M. G.; Waugh, J. *J. Chem. Phys.* **1972**, *59*, 569.
(47) Pines, A.; Gibby, M. G.; Waugh, J. *Chem. Phys. Lett.* **1972**, *15*, 373.
(48) Pople, J. A. *Proc. R. Soc.* **1957**, *A239*, 541.
(49) Schindler, M.; Kutzelnigg, W. *J. Chem. Phys.* **1982**, *76*, 1919.
(50) Schmidt-Rohr, K.; Spiess, H. W. *Multidimensional Solid State NMR and Polymers*; Academic Press: London, 1994.
(51) Schreckenbach, G.; Ziegler, T. *Chem. Rev.* **1991**, *91*, 651.
(52) Schuch, H.; Stehlik, D.; Hausser, K. H. *Z. Naturforsch.* **1971**, *26a*, 1944.
(53) Shepard, R.; Shavitt, I.; Simons, J. *J. Chem. Phys.* **1982**, *76*, 543.
(54) Stehlik, D. The Mechanism of Optical Nuclear Polarization. In *Excited States*; Academic Press: New York, 1977; Vol. 3.
(55) Stevens, R. M.; Pitzner, P. M.; Lipscomb, W. N. *J. Chem. Phys.* **1963**, *38*, 550.
(56) van Wüllen, C.; Kutzelnigg, W. *Chem. Phys. Lett.* **1993**, *205*, 563.
(57) Vauthier, E. C.; Comeau, M.; Odiot, S.; Eliszar, S. *Can. J. Chem.* **1988**, *66*, 1781.
(58) Veeman, W. S. *Progr. NMR Spectrosc.* **1984**, *16*, 193.
(59) Vieth, H. M.; Macho, V.; Stehlik, D. *J. Phys. Chem.* **1979**, *83*, 3435.
(60) Wolinski, K.; Hinton, J. F.; Pulay, P. *J. Am. Chem. Soc.* **1990**, *112*, 8251.